Sarah Y. Khoudair
Ali H. Khidhir

Department of Physics, College of Science, University of Baghdad, Baghdad, IRAQ

Design and Implementation of an E-shaped Patch Antenna for Portable Devices Treated with Nd:YAG Laser to optimize Bandwidth and Gain

This paper presents the design and implementation of an inverted E-shaped patch antenna with a 6.5x14.1 mm^2 size. The antenna operates at 3.55 and 3.8 GHz frequencies and incorporates a Nd:YAG laser treatment to improve performance. The reflection coefficient of the proposed antenna was evaluated and measured, revealing a |S11| value lower than -10 dB within the intended frequency ranges, which spanned from 3.3 to 3.92 GHz with a bandwidth of 622 MHz and from 3.51 GHz to 4.34 GHz with a bandwidth of 834 MHz. Additionally, the antenna exhibited a gain of 4.2 dBi. After undergoing treatment, the antenna acquired a bandwidth of 1000 MHz. It resonated at frequencies of 3.55 and 3.8 GHz and experienced an enhanced gain of 5.2 dBi. The results exhibited a high level of agreement between the measured and simulated data, with few discrepancies attributable to fabrication tolerances. These qualities highlight the potential of the Nd:YAG laser-treated inverted E-shaped antenna for enhancing effective wireless communication systems.

Keywords: Communications; Satellites; Telecommunications; Laser treatment
Received: 03 August 2024; **Revised:** 29 September 2024; **Accepted:** 06 October 2024

1. Introduction

Wireless networking requires higher bandwidth, gain, and a dependable connection to accommodate the increasing prevalence of online video streaming and multimedia devices [1]. Although intensive research is ongoing on 4G technology to enhance bandwidth for Long Term Evolution (LTE), the focus and interest have shifted towards the next 5G communication technology [2,3]. The inverted E-shaped antenna has become popular in wireless applications because of its small size, easy integration, and varied performance. The antenna configuration, distinguished by its distinctive E-shaped geometry, provides notable benefits in terms of bandwidth and gain, rendering it appropriate for a range of contemporary communication systems, such as mobile devices, Wi-Fi networks, and IoT applications. The complex configuration of the inverted E-shaped antenna enables precise control over the radiation pattern and improved impedance matching, both of which are essential for successful signal transmission and reception [4-7].

In recent years, there have been proposals for several microstrip patch antennas explicitly designed for frequencies ranging from 1.8 GHz to 5.6 GHz [8]. However, patch antennas have numerous benefits and can be used in everyday scenarios. Nevertheless, these tools have certain drawbacks, including limited bandwidth and gain. Therefore, multiple researchers have documented various methods to overcome these limitations, focusing on improving the impedance bandwidth [9-11]. These modifications involve the implementation of slots in the fundamental shapes [12], altering the geometry [13], or employing multi-layer approaches [14].

The efficiency of the inverted E-shaped antenna can be further enhanced through recent improvements by employing laser processing. Laser technology utilizes intense and coherent light to alter the antenna's material properties and shape. These factors can lead to improved surface roughness, increased conductivity, and enhanced dielectric characteristics, all contributing to higher antenna performance [15,16]. By accurately manipulating the laser characteristics, it becomes possible to make customized modifications that meet specific design criteria, resulting in antennas with increased gain and broader bandwidths [17-19].

Recently, researchers have concentrated on improving the efficiency of patch antennas to allow for operation across several frequency bands, achieve broader frequency ranges, and enhance signal gain [20-27]. The physical dimensions of the antenna are 60×55 mm^2. A different research [21] presents a patch antenna made of Teflon substrate that is specifically built for sub-6 GHz 5G. This antenna operates in three different frequency bands and has 50×80 mm^2 dimensions.

As described in [22], the air gap technique improves the performance of microstrip patch antennas operating at 2.4 GHz by introducing a 3 mm gap between the substrate and ground plane. This leads to an increase in gain from 7.1 dBi to 7.91 dBi. However, there is a trade-off between gain and bandwidth, as the bandwidth decreases from 110.7 MHz to 72.873 MHz. In the study mentioned in reference [23], a printed antenna was developed for the n77 and n78 bands of 5G New Radio (NR). The antenna used an FR-4 substrate with dimensions of 28×20 mm^2. It achieved a maximum gain of 2.5 dBi and a bandwidth of 700 MHz. The Defected Ground Structure (DGS) approach, as described in reference [24], allows for operation at

frequencies of 4.53 GHz and 4.97 GHz. This is achieved by utilizing a RO5880 substrate with a relative permittivity of 2.2. The method yields gains of 5 dBi and 4.57 dBi at these frequencies, respectively. However, the bandwidth is not indicated in the given information.

The paper [25] presents a patch antenna with a slotted plus shape design, employing a Rogers RT5880 substrate. This antenna is specifically designed for sub-6 GHz 5G applications at a frequency of 3.12 GHz. The antenna utilizes the Defected Ground Structure (DGS) approach to achieve frequency coverage. It has a bandwidth of 2.56 GHz and a gain of 2.44 dBi. According to the information provided in reference [26], a single-band antenna utilizes an Arlon AD300C substrate. This antenna operates at a frequency of 5.65 GHz and has a gain of 7.15 dBi.

Additionally, it has a bandwidth of 135 MHz. Finally, a microstrip patch antenna is described in [27]. This antenna utilizes slots and parasitic strips and operates at 3.45 and 5.9 GHz frequencies. It has gain of 3.83 dBi and 0.576 dBi and bandwidths of 160 and 220 MHz. The antenna is compact, with dimensions of 36 × 37 mm².

Recent developments include utilizing an Nd:YAG laser to improve antenna gain and bandwidth [28,29]. The laser treatment accurately alters the surface and structural features of the antenna, resulting in notable enhancements in electromagnetic performance by correcting its physical and microstructural characteristics.

This work involves designing and implementing an inverted E-shaped patch antenna that functions at 3.55 and 3.8 GHz frequencies. After the implementation process, the radiation line of the antenna is subjected to treatment using an Nd:YAG laser to enhance both the gain and bandwidth. Furthermore, the antenna incorporates an internal gap to optimize its performance. This technology provides a means to accomplish desirable improvements in antenna properties, facilitating the advancement of more efficient wireless networks. The comparative analysis reveals that the suggested design outperforms prior efforts regarding broader bandwidth, higher efficiency and gain, better impedance matching, and a compact profile.

2. Antenna Design

Figure (1a-d) displays the top and bottom views of the proposed design with a fabricated prototype of the inverted E-shaped patch antenna. The proposed system comprises an inverted-E antenna on a ground plane measuring 6.5x14.15 mm^2. The antenna is designed on an FR4 substrate with a thickness of 1.4 mm, a relative permittivity of 4.2, and a tangent loss of 0.025. The antenna is shorted with a rectangular shape connected to the ground and has an L-shaped parasitic radiator.

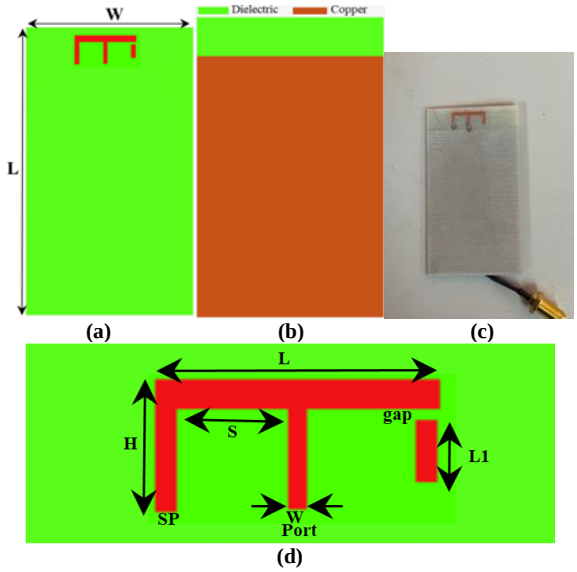

Fig. (1) Geometry of the proposed antenna: (a) Top view, (b) Bottom view, (c) prototype image and (d) Enlarged design with dimensions in mm: L=14.1, H=6.5, S=5.52, W=1, L1=3, gap=0.5, sp=short pin

Figure (2a-d) illustrates the antenna design process, providing a detailed representation of the sequential stages involved. During the first stage (step a), a 50-ohm microstrip line provides power to the antenna. Additionally, a stub is incorporated into the design to ensure impedance matching (step b). However, a problem develops because the surface beneath the radiating patch antenna has an uneven impedance, causing the antenna to not work well across all frequencies.

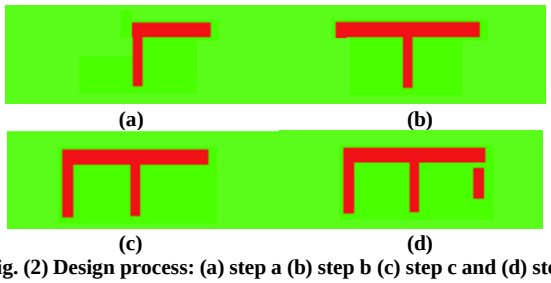

Fig. (2) Design process: (a) step a (b) step b (c) step c and (d) step d

A rectangular patch is added and attached to the ground plane beneath the radiator's edge to overcome this difficulty. This ensures that the feed line and the patch have the same impedance, resulting in a match. The significant enhancement can be noted in Fig. (2c), providing insight into step c of the process. Figure (2d) illustrates the next phase (step d) in the ongoing sequence, where an L-shaped parasitic element is attached to the primary radiator using a stub. This connection allows the primary radiator to operate in the higher frequency region. This configuration is vividly illustrated in Fig. (3), providing a visual explanation of this element.

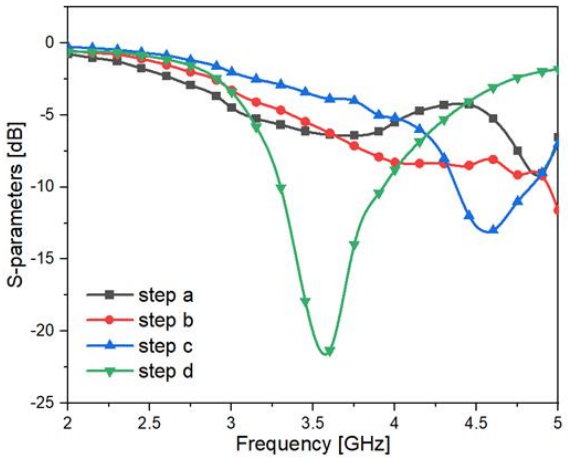

Fig. (3) Reflection coefficient for the design process

The methodology for determining the fundamental characteristics is explained using the transmission line model [30-39].

Step 1: Calculation of the patch width (W). The width of the microstrip patch antenna is determined by Eq. (1)

$$W = \frac{c}{2f_o}\sqrt{\frac{2}{\varepsilon_r+1}} \quad (1)$$

where $f_o$indicate the resonance frequency in GHz, c is the speed light, and ε_r is the relative permittivity of the substrate.

Step 2: Calculate the effective dielectric constant ε_{reff}

$$\varepsilon_{reff} = \frac{\varepsilon_r+1}{2} + \frac{\varepsilon_r-1}{2}\left(1+12\frac{h}{w}\right)^{-\frac{1}{2}} \quad (2)$$

where h is the substrate thickness

Step 3: Calculation of the effective length, denoted as

$$L_{eff} = \frac{c}{2f_o\sqrt{\varepsilon_{reff}}} \quad (3)$$

Step 4: Calculation of the length extension (ΔL)

$$\Delta L = \frac{(\varepsilon_{reff}+0.3)\left(\frac{w}{h}+0.264\right)}{(\varepsilon_{reff}-0.258)\left(\frac{w}{h}+0.8\right)} \quad (4)$$

Step 5: Calculate the precise patch length (La), which estimates to $L1 + gap + L$

$$La = L_{\text{eff}} - 2\Delta L \quad (5)$$

The antenna's design, shaped like an inverted E, was simulated and improved using a full-wave electromagnetic simulator called CST. Figure (4) displays the analysis of the reflection coefficient conducted by the CST tool. By referring to the datasheet and slightly adjusting the settings, the frequency resonates at 3.55 and 3.8 GHz.

3. Results and Discussions

The reflection coefficient of the manufactured antenna was simulated and tested using the Site Master (Anritsu S362E) and a vector network analyzer (VNA), as depicted in figures (5a,b). Figure (6a,b) displays the reflection coefficient plot comparing the simulated and measured data. The magnitude of the S11 parameter at the specified frequency range was less than -10 dB, while it exhibited resonance at 3.5 GHz with a bandwidth of 622 MHz (3.3-3.92 GHz). In addition, the antenna achieved a bandwidth of 834 MHz (from 3.51 to 4.34 GHz) while resonating at 5.8 GHz.

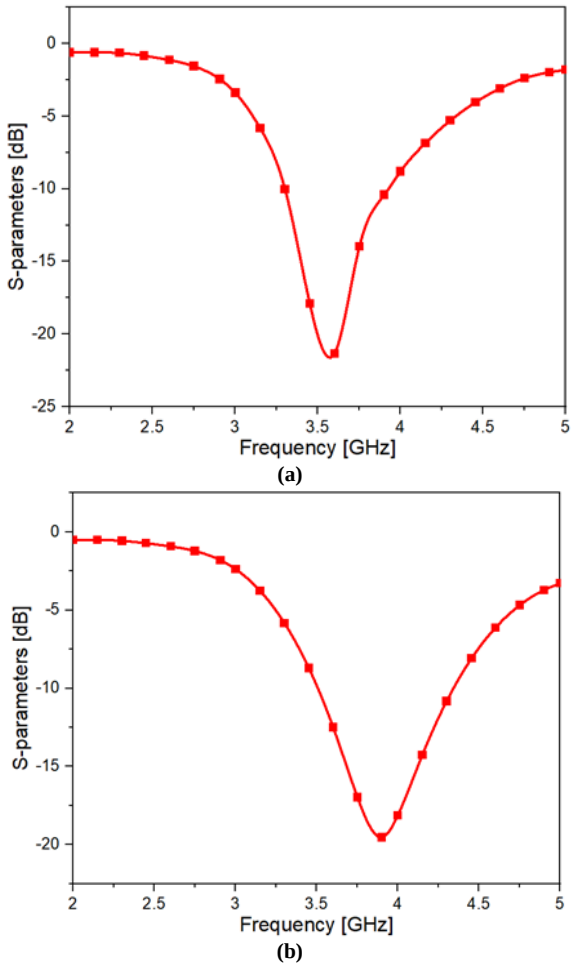

Fig. (4) Simulated reflection coefficients at (a) 3.55 GHz and (b) 3.8 GHz

By comparison, the recorded bandwidth measurements for the 3.5 GHz frequency range from 3.1 to 4.1 GHz, whereas those for the 3.8 GHz frequency range from 3.38 to 4.4 GHz. The simulated and measured results exhibited a high degree of agreement, with a minor discrepancy attributable to the fabrication tolerance and soldering loss.

The Voltage Standing Wave Ratio (VSWR) and the characteristic impedance are two crucial elements that determine the features of the proposed design. VSWR quantifies the effectiveness of transmitting radio-frequency power from a power source, through a transmission line, and into a load. The standing wave's maximum-to-minimum amplitude ratio is utilized to evaluate impedance matching in RF systems. Optimally, a VSWR of 1:1 signifies impeccable alignment, minimizing reflections, and power dissipation. The characteristic impedance refers to the intrinsic impedance of a transmission line, which is commonly 50 ohms in RF applications. It represents the

relationship between voltage and current of a single propagating wave.

(a) (b)

Fig. (5) Site Master and vector network analyzer

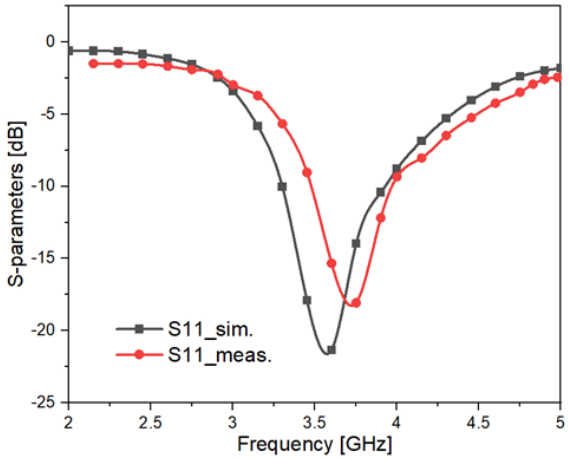

(a)

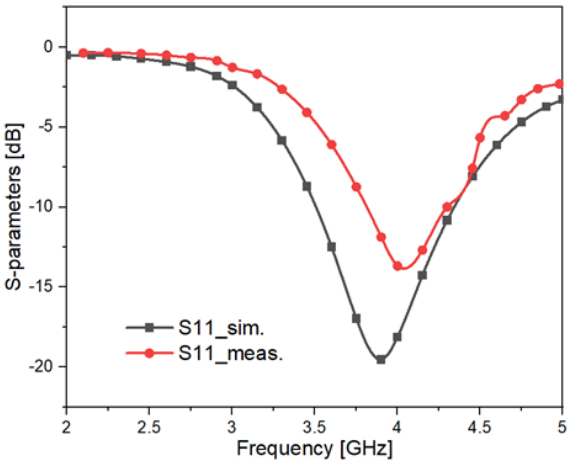

(b)

Fig. (6) Simulated and measured S11: (a) at 3.55 GHz and (b) at 3.8 GHz

Figures (7a,b) depict the VSWR and impedance values for the 3.55 and 3.8 GHz resonance frequencies. The VSWR values for both frequencies are less than 1, suggesting effective power transmission, and the impedance values are around 50 ohms, indicating satisfactory impedance matching.

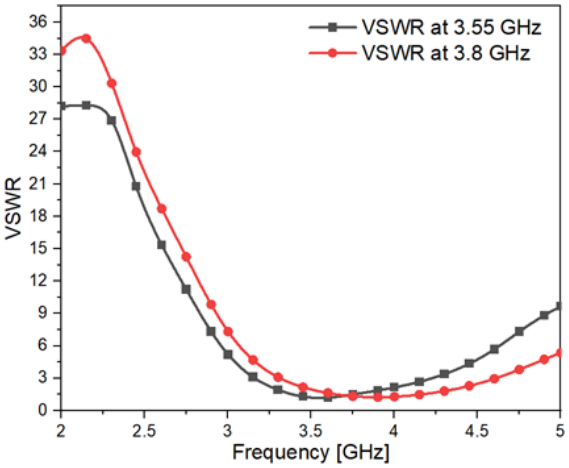

(a)

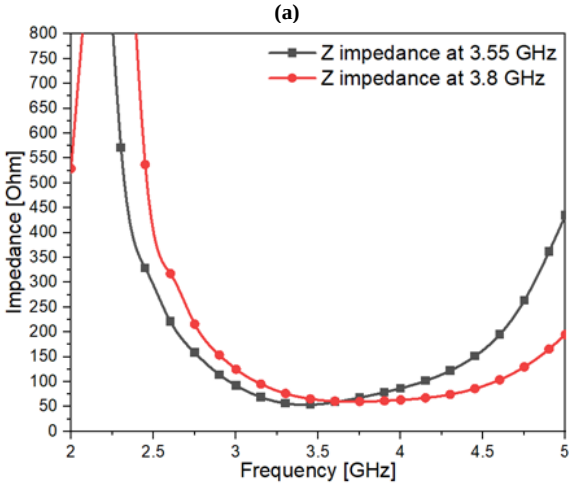

(b)

Fig. (7) (a) VSWR and (b) characteristics impedance

Before utilizing the Nd:YAG laser depicted in Figure 8 on the microstructure of the inverted E-shaped patch antenna installed on an FR-4 dielectric substrate, an analysis of particles indicates that the surface is generally clean and even, with limited particulate matter. The particles present are often of a very small size, commonly in the range of microns to sub-microns, as depicted in Fig. (9a,b). The standard roughness measurement in Fig. (10a) was conducted using atomic force microscopy (AFM). The results demonstrate low surface roughness parameters.

(a)

(b)

Fig. (8) Sample bombardment by Nd:YAG laser

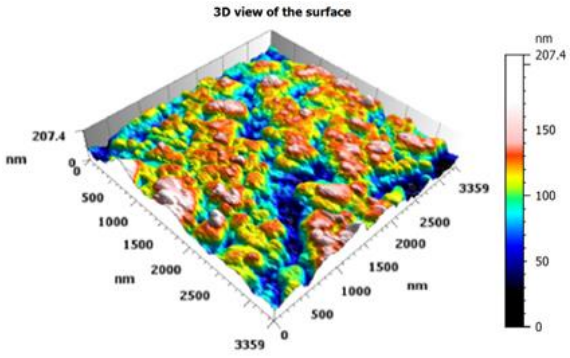

(a)

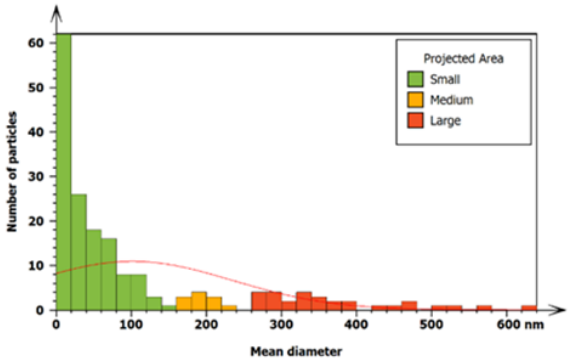

(b)

Fig. (9) Particle analysis before: (a) Microstructure of E-shaped patch antenna at fr=3.8 GHz before Nd:YAG laser treatment and (b) Histogram

After applying the Nd:YAG laser, notable alterations occur on the antenna's surface. The laser ablation process results in significant surface smoothness, defined by craters, ridges, and other topographical characteristics. This smoothness is caused by the material's melting, vaporization, and re-solidification, as depicted in Fig. (11a,b). The surface experiences non-uniformity in particle size and distribution as vaporized material condenses, forming debris particles of different sizes.

Examining roughness reveals a significant reduction in surface roughness parameters, such as Ra and Rq after the laser application. This indicates that the surface becomes smoothness, with lower prominent peaks, valleys, and general undulation, as depicted in Fig. (10b). The heightened smoothness impacts the characteristics of the material, such as its conductive layers and dielectric properties, because it alters the surface structure.

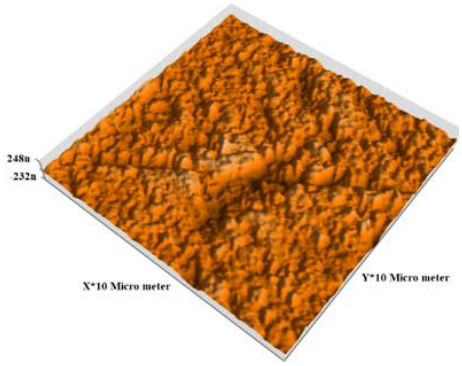

(a)

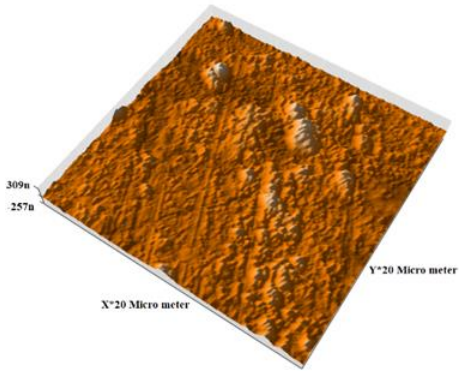

(b)

Fig. (10) Surface roughness: (a) before apply Nd:YAG laser treatment and (b) after at 3.8 GHz

Figure (12) compares the proposed antenna's measured and simulated scattering parameters with and without treatment, highlighting the discrepancy between them. The antenna provides a broad frequency range of 622 and 834 MHz without any modifications and has a resonance frequency of 3.55 and 3.8 GHz. The Nd:YAG laser, mounted atop the antenna, provides a broad frequency range of 1 GHz, from 3.1 to 4.1 GHz and 3.38 to 4.4 GHz. It exhibits resonances at 3.55 and 3.8 GHz, as depicted in Fig. (12). The measured and simulated results of the proposed antenna, both with and without treatment, exhibit a high level of agreement.

Figure (13) displays the gain vs frequency plot of the proposed antenna, both with and without treatment. The antenna exhibits a gain more significant than 4 dBi within the operational frequency range. At the resonance frequency of 3.55 GHz, the antenna achieves a peak gain of approximately 4.2 dBi, as depicted in Fig. (13). The treatment antenna's gain was increased by approximately 20%. We have a maximum gain of 5.2 dBi relative to an isotropic radiator. The plot demonstrates no substantial discrepancies between the measured and projected findings.

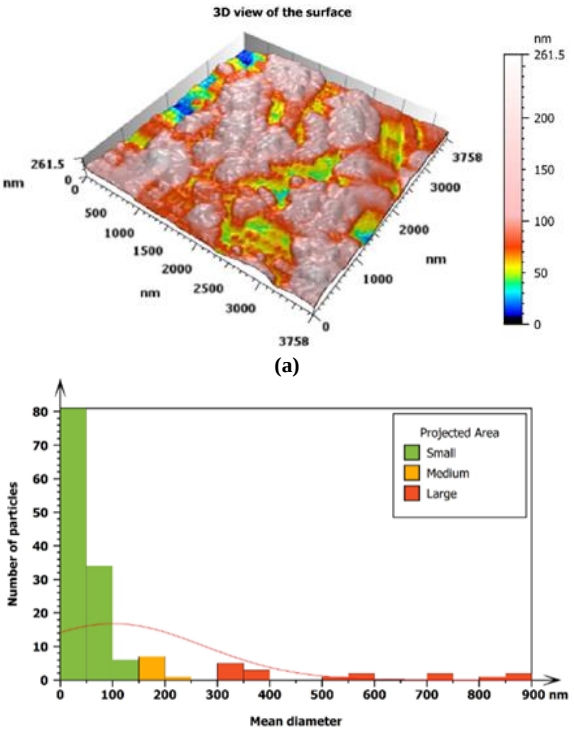

(a)

(b)

Fig. (11) Particle analysis After: (a) Microstructure of E-shaped patch antenna at f_r=3.8 GHz After Nd:YAG laser treatment and (b) Histogram

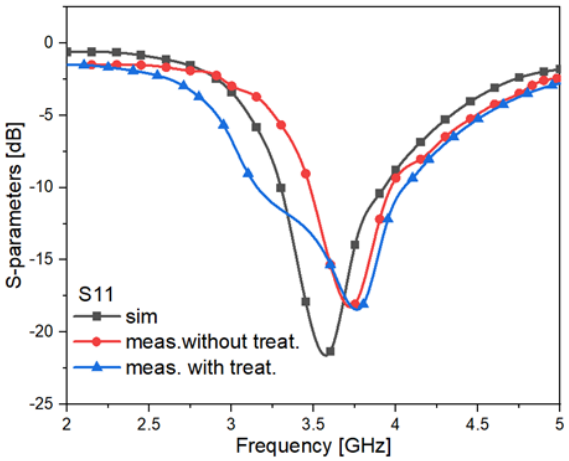

(a)

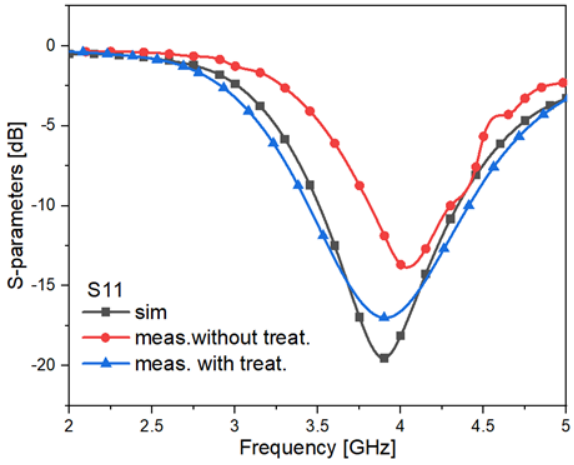

(b)

Fig. (12) Reflection coefficient with and without treatment: (a) simulated (b) measured without treatment

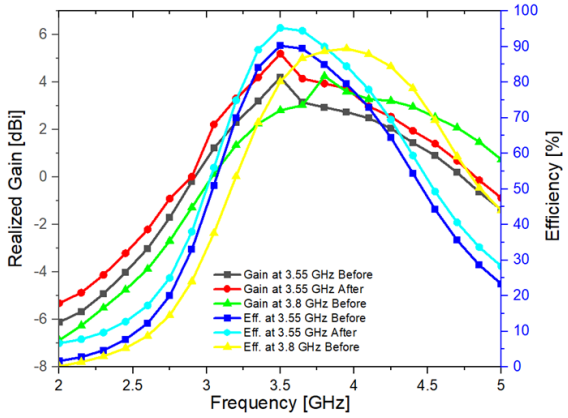

Fig. (13) Antenna gain and efficiency at 3.55 and 3.8 GHz

Also, figure (13) displays the proposed antenna's radiation efficiency. The antenna has a more than 85% radiation efficiency within its working bandwidth. The efficiency reaches 88% and 90% at 3.55 GHz and 3.8 GHz resonance frequencies, respectively. A marginal enhancement in radiation efficiency is detected upon loading the Nd:YAG. The laser-loaded antenna demonstrates a radiation efficiency exceeding 90% within its operational bandwidth, with peak values reaching 95% at a frequency of 3.55 GHz, as depicted in Fig. (13).

Figure (14) shows the radiation pattern of the three-dimensional electric field at two frequencies, namely 3.55 and 3.8 GHz. The magnitude of the E-field pattern is 17.9 V/m, corresponding to a peak gain of 4.2 dBi.

Figure (15) depicts the radiation pattern of the recommended E-shaped antenna in two dimensions at resonance frequencies of 3.55 and 3.8 GHz without any treatment applied. The antenna design allows for bidirectional radiation in the E-plane at both frequencies and omnidirectional radiation in the H-plane at both operational frequencies. The radiation pattern exhibits a butterfly-shaped configuration, preferable for the electric field (E-field).

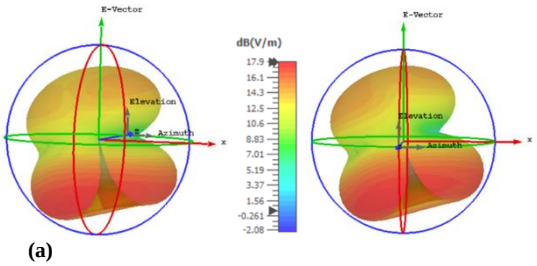

(a) (b)

Fig. (14) 3D radiation pattern at two frequencies: (a) at 3.55 GHz and (b) at 3.8 GHz

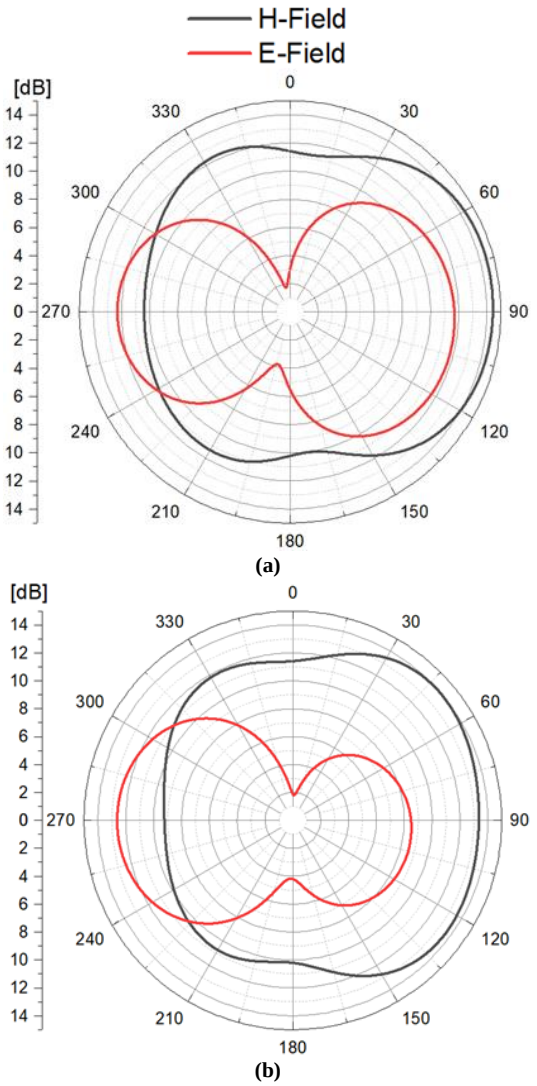

(a)

(b)

Fig. (15) 2-D Electric and magnetic fields at (a) 3.55 GHz and (b) at 3.8 GHz

Table (1) compares the proposed work and the references under consideration. The results demonstrate that the suggested configuration provides higher performance. The present design exhibits a wide frequency range (622 and 834 MHz), high efficiency (over 88%), high gain (>5 dBi), impedance matching near 50 Ω, and a compact form factor (6.5x14.15 mm²), all of which are comparable to the sources mentioned in table (1). Furthermore, the VSWR value is around 1, as depicted in Fig. (7), suggesting little reflected waves and a virtually perfect match in the transmission line.

4. Conclusion

The utilization of the Nd:YAG laser treatment has demonstrated its effectiveness in enhancing antenna performance, enabling precise manipulation of material and geometric characteristics. This approach improves the antenna's physical characteristics and provides advantageous microstructural modifications, enhancing operational efficiency. The results show substantial enhancements in bandwidth and gain, with initial bandwidths of 622 and 834 MHz and, after treatment, a bandwidth of 1000 MHz. The measured and calculated reflection coefficients demonstrated a |S11| value lower than -10 dB within the desired frequency ranges, verifying the efficiency of the design and treatment.

References

[1] M.A. Jensen and J.W. Wallace, "A review of antennas and propagation for MIMO wireless communications", *IEEE Trans. Antennas Propag.*, 52(11) (2004) 2810-2824.

[2] Q.H. Kareem, R.A. Shihab and H.H. Kareem, "Compact dual-polarized reconfigurable MIMO antenna based on a varactor diode for 5G mobile terminal applications", *Prog. Electromag. Res. C*, 137 (2023) 185-198.

[3] J.G. Andrews et al., "What Will 5G Be?", *IEEE J. Sel. Areas Commun.*, 32(6) (2014) 1065-1082.

[4] Y. Ge and T. S. Bird, "E-shaped patch antennas for high-speed wireless networks," *IEEE Trans. Antennas Propag.*, 52 (2004).

[5] M.T. Ali et al., "E-shaped microstrip patch antenna for wideband application," 2011 *IEEE Int. RF Microwave Conf. Malaysia*, 12-14 December 2011, Seremban, Malaysia, pp. 439-443.

[6] H. Malekoor and S. Jam, "Miniaturized asymmetric E-shaped microstrip patch antenna with folded patch feed", *IET Microwave Antennas Propag.*, 7(2) (2013) 85-91.

[7] K. Praveen Kumar et al., "The effect of dielectric permittivity on radiation characteristics of coaxially fed rectangular patch antenna: Design & analysis", *Int. J. Adv. Res. Computer Commun. Eng.*, 2(2) (2013) 1254-1258.

[8] K. Mazen et al., "Design of multi-band microstrip patch antennas for mid-band 5G wireless communication," *IET Microwave Antennas Propag.*, 12(5) (2021) 459-469.

[9] P.S. Nakar, "Design of a compact microstrip patch antenna for use in wireless/cellular devices", MSc thesis, Florida State University, USA (2004).

[10] B. Analui and A. Hajimiri, "Bandwidth enhancement for transimpedance amplifiers", *IEEE J. Solid-State Circ.*, 39(8) (2004) 1263-1270.

[11] V.T. Rathod, "A review of electric impedance matching techniques for piezoelectric sensors, actuators and transducers", *Eng.*, 8(2) (2019)169-2019.

[12] D.A. Stephenson and J.S. Agapiou, **"Metal Cutting Theory and Practice"**, CRC Press (FL, 2018), Ch. 2, p. 45.
[13] M.B. Prime, "Cross-sectional mapping of residual stresses by measuring the surface contour after a cut", *J. Eng. Mater. Technol.*, 123(2) (2001) 162-168.
[14] J. Balster et al., "Multi-layer spacer geometries with improved mass transport", *J. Membrane Sci.*, 282(1-2) (2006) 351-361.
[15] A.V. Kildishev et al., "Numerical modeling of plasmonic nanoantennas with realistic 3D roughness and distortion", *Sensors*, 11(7) (2011) 7178-718.
[16] M. Ghanim et al., "Highly Directive Hybrid Yagi-Uda Nanoantenna for Radiation Emission Enhancement", *IEEE Photon. J.*, 8(5) (2016) 1–12.
[17] Y. Ikeda and R. Tsuruoka, "Characteristics of microwave plasma induced by lasers and sparks", *Appl. Opt.*, 51 (2012) 183-191.
[18] Y.-F.C. Chau et al., "Tunable Optical Performances on a Periodic Array of Plasmonic Bowtie Nanoantennas with Hollow Cavities", *Nanoscale Res. Lett.*, 11(1) (2016) 411.
[19] J. Hayashi et al., "Effects of Microwave-Enhanced Plasma on Laser Ignition", *in Proc. Int. Conf. Ignition Sys. Gasoline Engines, Berlin, Germany*, 3-4 (2016) 245-253.
[20] A.S. Mekki et al., "Gain Enhancement of a Microstrip Patch Antenna Using a Reflecting Layer", *Int. J. Antennas Propag.*, 2015(1) (2015) 975263.
[21] X. Tang et al., "Ultra-Wideband Patch Antenna for Sub-6 GHz 5G Communications", *in Proc. 2019 Int. Workshop on Electromagnetics: Appl. Student Innov. Compet. (iWEM), Qingdao, China*, 18–20 (2019) 5–7.
[22] K.W.S. Al Kharusi et al., "Gain enhancement of rectangular microstrip patch antenna using air gap at 2.4 GHz", *Int. J. Nanoelectron. Mater.*, 13 (2020) 211–224.
[23] A. Kapoor et al., "Compact wideband-printed antenna for sub-6 GHz fifth-generation applications", *Int. J. Smart Sensor Intell. Sys.*, 13 (2020) 1–10.
[24] M.F.A. Sree, M.H.A. Elazeem and W. Swelam, "Dual Band Patch Antenna Based on Letter Slotted DGS for 5G Sub-6GHz Application", *J. Phys.: Conf. Ser.*, 2128(1) (2021) 012008.
[25] L.C. Paul et al., "A slotted plus-shaped antenna with a DGS for 5G Sub-6 GHz/WiMAX applications", *Heliyon*, 8 (2022) 12040.
[26] M. Kösem and Tütüncü, "Substrate Analysis on the Design of Wide-Band Antenna for Sub-6 GHz 5G Communication", *Wireless Personal Commun.*, 125 (2022) 1523–1535.
[27] S.K. Noor et al., "A Patch Antenna with Enhanced Gain and Bandwidth for Sub-6 GHz and Sub-7 GHz 5G Wireless Applications", *Electronics*, 12(12) (2023) 2555.
[28] R. Taubert et al., "3D optical Yagi–Uda nanoantenna array", *Nature Commun.*, 2 (2011) 267.
[29] L. Novotny and N. van Hulst, "Antennas for light", *Nature Photonics*, 5(2) (2011) 83–90.
[30] A.J. Mohamed et al., "Design and Implementation of a Multi-Band Quad-Port MIMO Antenna for the 5G Applications", *in Proc. 2023 Second Int. Conf. Adv. Computer Appl. (ACA), Misan, Iraq*, (2023) 1-6.
[31] L.W. Abdullah, Q.H. Kareem and A.H. Sallomi, "A quadport multiple-input-multiple-output system for underlay or interweave cognitive radio", *Indonesian J. Electr. Eng. Computer Sci.*, 29(3) (2023) 1480-1495.
[32] A.H. Khidhir, "Implementation of a Circular Shape Patch Antenna at 2.4 GHz for Different Wireless Communications", *Iraqi J. Sci.*, 64(1) (2023) 204-214.
[33] A.M. Abdulhussein, A.H. Khidhir and A.A. Naser, "Omnidirectional Microstrip Patch Antenna for 2.4 GHz Wireless Communications", *J. Phys.: Conf. Ser.*, 2114(1) (2021) 012051.
[34] A.H. Khidhir, "Dual-band Rectangular Microstrip Patch Antenna for WiMAX Wireless Communications by Chemical Method", *J. Phys.: Conf. Ser.*, 2114(1) (2021) 012022.
[35] A.M. Abdulhussein, A.H. Khidhir and A.A. Naser, "2.4 GHz Microstrip Patch Antenna for S-Band Wireless Communications", *J. Phys.: Conf. Ser.*, 2114(1) (2021) 012029.
[36] A.M. Abdulhussein, A.H. Khidhir and A.A. Naser, "Design and Implementation of Microstrip Patch Antenna Using Inset Feed Technique for 2.4 GHz Applications", *Int. J. Microwave Opt. Technol.*, 16(4) (2021) 355–361.
[37] A.H. Khidhir, "Optimum diameter for laser beam and effect of temperature rise on the optical bistability hysteresis loops", *Iraqi J. Phys.*:18(45) (2020) 32-39.
[38] A.H. Khidhir, "Study of optical bistability in fully optimized laser Fabry-Perot system", *Iraqi J. Phys.*, 16(39) (2018) 152-161.
[39] A. H. Khidhir, "Dynamic Response of a Nonlinear Fabry-Perot Etalon for Various Medium Response Times", *Baghdad Sci. J.*, 17(1) (2020) 120-125.

Table (1) Comparison of the proposed work and the references under consideration

Ref.	Antenna size (mm^2)	Frequency (GHz)	Bandwidth (MHz)	Gain (dBi)	Efficiency (%)
[20]	60x55	2.39	44.7	5.2	58
[21]	50x80	2.55, 3.5	2920	2.5, 3.05	-
[22]	80x80	2.4	72.8	7.9	79
[23]	28x20	3.65	700	2.5	
[24]	77x70	4.5, 4.97	-	5, 4.5	60
[25]	20x35	3.12	2560	2.44	90
[26]	53x55	5.65	135	7.13	62
[27]	36x37	3.45, 5.9	160, 220	3.8, 0.53	59
This work	6.5x14.1	3.55, 3.8	622, 834, 1000	4.2, 5.2	95

